Synthesis and characterization of Fe-doped aluminosilicate nanotubes with enhanced electron conductive properties

Shafia, Ehsan; Esposito, Serena; Bahadori, Elnaz; Armandi, Marco; Manzoli, Maela; Bonelli, Barbara. Synthesis and characterization of Fe-doped aluminosilicate nanotubes with enhanced electron conductive properties. JOURNAL OF VISUALIZED EXPERIMENTS. 2016 (117) pp: 1-14. DOI: 10.3791/54758

TITLE:

Synthesis and characterization of Fe-doped aluminosilicate nanotubes with enhanced electron conductive properties

AUTHORS:

Shafia, Ehsan

Department of Applied Science and Technology

Politecnico di Torino

Turin, Italy

ehsan.shafia@polito.it

Esposito, Serena

Department of Civil and Mechanical Engineering

Università degli Studi di Cassino e del Lazio Meridionale

Cassino,Italy

s.esposito@unicas.it

Bahadori, Elnaz

Department of Applied Science and Technology

Politecnico di Torino

Turin, Italy

elnaz.bahadori@polito.it

Armandi, Marco

Department of Applied Science and Technology

Institute of Chemistry

Politecnico di Torino

Turin, Italy

marco.armandi@polito.it

Manzoli, Maela

Department of Chemistry & NIS Interdepartmental Centre

University of Turin

Turin, Italy

maela.manzoli@unito.it

Bonelli, Barbara

Department of Applied Science and Technology & INSTM Unit of Torino-Politecnico

Institute of Chemistry

Politecnico di Torino

Turin, Italy

barbara.bonelli@polito.it

CORRESPONDING AUTHOR:

Barbara Bonelli

KEYWORDS:

Nanotubes, Fe-doping, band-gap lowering, sol-gel synthesis, nanomaterials characterization, imogolite, aluminosilicate, azo-dyes, adsorption, ζ-potential, Fe_2O_3 clusters, isomorphic substitution.

SHORT ABSTRACT:

Here, we present a protocol to synthesize and characterize Fe-doped aluminosilicate nanotubes. The materials are obtained by either sol-gel synthesis upon addition of $FeCl_3$*$6H_2O$ to the mixture containing the Si and Al precursors or by post-synthesis ionic exchange of preformed aluminosilicate nanotubes.

LONG ABSTRACT:

The goal of the protocol is to synthesize Fe-doped aluminosilicate nanotubes of the imogolite type with formula $(OH)_3Al_{2-x}Fe_xO_3SiOH$. Doping with Fe aims at lowering the band gap of imogolite, an insulator with chemical formula $(OH)_3Al_2O_3SiOH$, and at modifying its adsorption properties towards azo-dyes, an important class of organic pollutants of both wastewater and groundwater.

Fe-doped nanotubes are obtained by two ways: by direct synthesis where $FeCl_3$ is added to an aqueous mixture of the Si and Al precursors, and by post-synthesis loading where preformed nanotubes are contacted with a $FeCl_3$*$6H_2O$ aqueous solution. By both synthesis methods, isomorphic substitution of Al^{3+} by Fe^{3+} occurs still preserving the nanotube structure. Isomorphic substitution is indeed limited to *ca.* 1.0 wt. % Fe, since at higher Fe content (*i.e.* 1.4 % wt. Fe) Fe_2O_3 clusters form, especially when the loading procedure is adopted. The physico-chemical

properties of the materials are studied by means of X-ray powder diffraction (XRD), N_2 sorption isotherms at -196 °C, high resolution transmission electron microscopy (HRTEM), diffuse reflectance (DR) UV-Vis spectroscopy, and ζ-potential measurements. The most relevant result is the possibility to replace Al^{3+} ions (located at the outer surface of nanotubes) by post-synthesis loading on preformed imogolite without perturbing the delicate hydrolysis equilibria occurring during nanotubes formation. During the loading procedure, anionic exchange occurs where Al^{3+} ions at the outer surface of nanotubes are replaced by Fe^{3+} ions. In Fe-doped aluminosilicate nanotubes, isomorphic substitution of Al^{3+} by Fe^{3+} is found to affect the band gap of doped imogolite; nonetheless, Fe^{3+} sites at the outer surface of nanotubes are able to coordinate organic moieties, like the azo-dye Acid Orange 7, through a ligand-displacement mechanism occurring in aqueous solution.

INTRODUCTION:

The term nanotube (NT) is universally associated with carbon nanotubes,[1] one of the most studied chemical objects today. Less known is the fact that also aluminosilicate NTs can be synthesized,[2,3] besides being present in nature (mainly in volcanic soils). Imogolite (IMO) is a hydrated aluminosilicate with formula $(OH)_3Al_2O_3SiOH$[4,5] occurring as single-walled NTs with Al(OH)Al and Al-O-Al groups at the outer surface, and non-interacting silanols (SiOH) at the inner one.[6] Concerning geometry, the length varies from a few nm to several hundred nm;[3,5,7] the inner diameter is constant at 1.0 nm,[5] whereas the outer diameter is *ca.* 2.0 nm in natural IMO, increasing to 2.5-2.7 nm in samples synthetized at 100 °C: synthesis at 25°C yields, instead, NTs with an outer diameter close to that of natural IMO.[8] Recently, it has been shown that NTs with different external diameter may be also obtained by changing the acid used during the synthesis.[9]

In the dry powder, IMO NTs arrange in bundles with nearly hexagonal packing (Figure 1). Such an array of NTs gives rise to three kinds of pores,[10,11] and related surfaces.[12] Besides proper intra-tubes pores A (1.0 nm in diameter), smaller pores B (0.3-0.4 nm wide) occur among three aligned NTs within a bundle, and, finally, larger pores C occur as slit-mesopores among bundles (Figure 1). Both chemical composition and pore dimension affect the adsorption properties of the material: the surface of pores A is very hydrophilic, being lined by SiOH, and able to interact with vapors and gases like H_2O, NH_3 and CO.[12] Being very small, pores B are hardly accessible even to small molecules like water,[10,11] whereas pores C may interact with larger molecules, like phenol[6] and 1,3,5-triethylbenzene.[12] Amara *et al.* have recently shown that hexagonalization of NTs organized in closed-packed bundles occurs with (imogolite analogue) aluminogermate NTs:[13] this phenomenon, though not observed so far with aluminosilicate NTs, could affect accessibility of pores B, as well.

The interest in IMO-related chemistry has spread recently, one reason being the possibility of changing the composition of both the inner and outer surface of NTs. The presence of a plethora of hydroxyls renders IMO extremely sensitive to thermal degradation, since dehydroxylation occurs above 300 °C[6,14-16] with consequent NTs collapse.

The inner surface may be modified by several methods, including the substitution of Si atoms by Ge atoms,[17] with formation of either single or double walled[18] NTs with formula $(OH)_3Al_2O_3Si_{1-x}Ge_xOH$.[19] Post-synthesis grafting of organic functionalities leads to formation of NTs with formula $(OH)_3Al_2O_3SiO$-R, where R is the organic radical.[20] By one-pot synthesis in the presence of a Si precursor containing one organic radical directly linked to the Si atom, formation hybrid NTs form having formula $(OH)_3Al_2O_3Si$-R (R = $-CH_3$, $-(CH_2)_3-NH_2$).[21,22]

Modification of the outer surface is of paramount interest for the fabrication of imogolite/polymer composites,[23] and involves either electrostatic interaction or covalent bonding. The former method is based on the charge matching between the outer surface of NTs and a proper counter-ion, *e.g.* octadecylphosphonate;[24,25] the latter method implies a reaction between pre-formed IMO NTs and an organosilane, *e.g.* 3-aminopropylsilane.[26]

In water, electrostatic interaction between IMO and ions is possible due to the following equilibria:[27]

$Al(OH)Al + H^+ = Al(OH_2)^+Al$ (1)

$SiOH = SiO^- + H^+$ (2)

leading to charged surfaces that have been tested in the anions/cations retention from polluted water.[28-32]

The present work concerns yet another modification of the outer surface, *i.e.* the isomorphic substitution of (octahedral) Al^{3+} by Fe^{3+}, hereafter referred to as Al^{3+}/Fe^{3+} IS. This phenomenon is indeed common in minerals, whereas less is known about Al^{3+}/Fe^{3+} IS in IMO NTs.

Concerning doping, the first issue is the total amount of iron that can be hosted by the NTs without causing severe structural strains: a pioneering experimental work on Fe-doped IMO showed that NTs do not form at Fe contents higher than 1.4 wt % .[33] Successive theoretical calculations showed that Fe could either isomorphically substitute for Al or create "defective sites".[34] Such defects, *i.e.* iron oxo-hydroxide clusters, were supposed to reduce the band gap of IMO (an electrical insulator)[34,35] from 4.7 eV to 2.0-1.4 eV.[34] Accordingly, we have recently shown that the presence of Fe^{3+} imparts the solid new chemical and solid-state properties, lowering the band gap of IMO (E_g = 4.9 eV) to 2.4-2.8 eV.[36]

A recent report on Fe-doped aluminum-germanate NTs, isostructural with IMO, showed that actual Al^{3+}/Fe^{3+} IS is limited to 1.0 wt % Fe, since formation of iron oxo-hydroxides particles unavoidably occurs at higher Fe content, due to the natural tendency of Fe to form aggregates.[37] Similar results were obtained with Fe-doped IMO NTs.[33,36,38-40]

From the scientific point of view, the determination of the state of Fe and of its possible reactivity and adsorption properties in Fe-doped IMO is an important issue, which requires several characterization techniques.

In this work, we report the synthesis and characterization of Fe-doped IMO: two samples were synthesized with 1.4 wt % Fe content, by either direct synthesis (Fe-x-IMO) or post-synthesis loading (Fe-L-IMO); a third sample with a lower iron content (corresponding to 0.70 wt %) was obtained by direct synthesis, in order to avoid clusters formation and to obtain a material in which mostly Al^{3+}/Fe^{3+} IS occurred. In such a case, formation of NTs having chemical formula $(OH)_3Al_{1.975}Fe_{0.025}O_3SiOH$ is expected. Morphological and textural properties of the three Fe-doped IMO are compared to those of proper IMO. In addition, surface properties related to Fe(OH)Al groups are studied in water, by measuring the ζ potential and the interaction with the (bulky) anion of the azo-dye Acid Orange 7 (NaAO7), a model molecule of azo-dyes, an important class of pollutants of both wastewater and groundwater.[41] $AO7^-$ structure and molecular dimensions are reported in Figure 2a, along with the UV-Vis spectrum (Figure 2b) of a 0.67 mM water solution (natural pH = 6.8): in virtue of its molecular dimensions,[42] $AO7^-$ species should mainly interact with the outer surface of NTs, limiting parasitic interactions possibly deriving from diffusion within IMO inner pores, and it can be used as a probe molecule of the outer surface.

PROTOCOL:

1. Synthesis of 3 gr of IMO NTs

1.1. In a dry-box, prepare a 80 mM $HClO_4$ solution by slowly adding 1.3 mL of perchloric acid 70 wt. % to 187.7 mL of double distilled water at room temperature (r.t.). Use a 2000 mL beaker that will be useful for successive dilution (step 1.6).

1.2. In a smaller beaker within the dry-box, mix 8 mL of aluminum-tri-*sec*-butoxide (97%) (ATSB, as source of aluminum)[43,44] and 3.8 mL tetraethyl orthosilicate (98%) (TEOS, as source of Si) in the molar ratio Al:Si = 2 : 1.1. Use graduated pipettes to measure reagents volumes.

1.3. Leave the mixture under mild stirring for one min, until a clear and uniform mixture (without any suspended solid particles) is obtained.

1.4. Immediately after, with a Pasteur pipette dropwise add the whole mixture to the aqueous solution of $HClO_4$ under stirring (the final molar ratios are Si : Al : $HClO_4$ = 1.1 : 2 : 1). By adding the mixture to the $HClO_4$ aqueous solution, white clusters form and pH increases to 5.

1.5. Stir the final mixture at r.t. for about 18 hr, until a transparent solution is obtained.

1.6. Under stirring, add 1.3 L of double distilled water (measured with a graduated cylinder)

to dilute the solution to 20 mM with respect to Al. Stir the obtained 20 mM Al solution for about 20 min.

1.7. Pour the mixture into a polytetrafluoroethylene autoclave (with thick walls) and leave it within a stove for 4 days at 100 °C without stirring.

1.8. After 4 days, filter the clear and transparent solution (use a 0.02 micron filter) to collect the NTs and wash with double distilled water, obtaining a dense, transparent mixture.

1.9. Dry the mixture in a stove at 50-60 °C for 1 day. The final IMO powder has a white color.

2. **Synthesis of 3 gr Fe-x-IMO NTs (with either 0.70 or 1.4 % wt. Fe)**

2.1. In a dry-box, prepare a 80 mM solution of $HClO_4$ by slowly adding 1.3 mL of perchloric acid 70 wt. % to 187.7 mL of double distilled water (pH = 1.0). Use a 2000 mL beaker that will be useful for successive dilution (step 2.6).

2.2. Dissolve 0.1 gr of $FeCl_3*6H_2O$ in the so-obtained $HClO_4$ acid solution to obtain Fe-0.70-IMO NTs.

2.3. Dropwise add 8 mL ATSB and 3.8 mL TEOS into the iron-containing solution. Use graduated pipettes to measure reagents volumes. Check that pH is equal to 4. Leave the mixture

under stirring at r.t. for 18 hr.

2.4. After 18 h, dilute the resulting solution to 20 mM in Al by adding 1.3 L of double-distilled water (measured with a graduated cylinder) and maintain it under stirring for 1 h. Afterwards, pour it inside a sealed polytetrafluoroethylene autoclave (with thick walls) and leave it within a stove for 4 days at 100 °C

2.5. Filter the solution, wash the resulting reddish-brown powder with bi-distilled water and dry overnight at 50 °C in oven.

2.6. In order to prepare Fe-1.4-IMO NTs, repeat all the steps with 0.2 gr of $FeCl_3*6H_2O$.

3. Synthesis of Fe-L-IMO NTs.

3.1. Disperse 0.25 g IMO in 15 mL double distilled water.

3.2. Add 0.025 g $FeCl_3*6H_2O$ to the mixture (weight calculated considering a slight excess of iron(III) chloride hexahydrate). Leave under stirring for 18 hr: after 18 hr stirring, the colour of the mixture turns from yellow to reddish brown indicating the initial formation of iron oxo/hydroxide species.

3.3. Add 3.0 mL water and 1.5 mL NH_4OH solution (33% by weight) to precipitate all Fe^{3+} species as oxo/hydroxide.

3.4. Filter the mixture, wash the resulting powder with double-distilled water and dry in stove at 120 °C for 48 hr.

4. Sample characterization

4.1. Before measuring low angles X-ray diffraction (XRD) patterns of the sample, mill 100 mg of powder in an agate mortar, deposit it on a sample holder, and press it with care in order to get a uniform and smooth surface. Instrumental parameters of XRD patterns here reported are detailed in ref. 36.

4.2. To obtain high resolution electron transmission microscopy (HRTEM) micrographs, mill 10 mg of powder in an agate mortar. In order to obtain a well-dispersed sample for HRTEM inspection, contact milled powder with a Cu grid covered with a Lacey carbon film, and remove the excess by gently shaking the grid, in order to leave only few grains electrostatically interacting with the sample holder. Avoid dispersing the powder in a solvent, which could modify NTs arrangement. Instrumental parameters of HRTEM measurements here reported are detailed in ref. 36 and 39.

4.3. To determine BET SSA (Brunauer-Emmett-Teller Specific Surface Area) and porous volume values reported in Table 1, measure N_2 adsorption/desorption isotherms at -196°C. Before measurement, outgas the samples at 250 °C, in order to remove water and other atmospheric contaminants,[10] still preserving NTs.[6,14-16] Instrumental details are reported in ref.

39.

4.4. Outgas the powder in a UV-Vis quartz cell connected to a standard vacuum frame (residual pressure below 10^{-3} mbar) and take its diffuse reflectance (DR) UV-Vis spectrum. Instrumental parameters of DR-UV-Vis spectra here reported are detailed in ref. 36.

4.5. Experimental and instrumental details concerning electrophoretic mobility measurements are reported in ref. 39.

4.6 NaAO7 adsorption experiments

4.6.1. Prepare 200 mL of 0.67 mM NaAO7 solution by adding double distilled water to 0.047 g NaAO7 in a volumetric flask. The solution pH is 6.80.

4.6.2. Pour 50 mL of the solution inside a dark bottle, and add 50 mg of IMO (powder concentration 1g L^{-1}). Keep the solution under stirring during the experiment. Repeat this step with the other powders (powder concentration 1g L^{-1}).

4.6.3. At regular time intervals (t: 0 sec, 5 min, 10 min, 45 min, 2hr, 5 hr, 24 hr and 72 hr), recover 5 mL of the supernatant by centrifugation at 835 x g for 3 min.

4.6.4. Analyze the supernatant by transmission UV-Vis spectroscopy in a 1 mm path cuvette. In water, $AO7^-$ undergoes azo-hydrazone tautomerism, whereas the hydrazone form is stable in the solid phase, as shown by the UV-Vis spectrum in Figure 2b. Determine the amount of $AO7^-$

removed from the solution by measuring the decrease of the 484 nm band intensity of the hydrazone form, according to the literature.[38,39,41]

REPRESENTATIVE RESULTS

Concerning the synthesis of IMO and Fe-doped IMO NTs the most relevant issues are i) the formation of NTs, especially during Fe-doping by direct synthesis; ii) the actual environment of Fe species in the final materials and iii) the effect of Fe on the physico-chemical properties of the material, especially its band gap and its adsorption properties. The presence of Fe at the outer surface of NTs is indeed expected to modify the interactions between the NTs and adsorbate species, especially in water solution. The above aspects have to be assessed by multiple characterization techniques. DR-UV-Vis spectroscopy is used to assess the coordination of iron species in doped samples, as well as the presence of isolated Fe^{3+} sites and/or iron oxo-hydroxide clusters. ζ-potential measurements allow studying the surface charge of the samples in aqueous environment, and adsorption of $AO7^-$ to assess the behavior of the material for towards an azo-dye used as a probe of NTs external surface.

The successful synthesis of NTs is documented by XRD patterns, along with HRTEM analysis: all the samples showed the typical XRD pattern ascribable to NTs organized in a hexagonal array (Figure 3a).[43] The main peak corresponds to the d_{100} reflection, from which the cell parameter, which corresponds to the center-to-center distance between two aligned NTs in a hexagonal packing (Figure 1), is calculated as $a = 2d_{100}/\sqrt{3}$. The d_{100} peak is in the same position ($2\theta = 3.88$ °) with both IMO and Fe-L-IMO, whereas it shifts to slightly higher angles with samples prepared by direct synthesis, leading to a decrease in the corresponding values of both d_{100} and a. This phenomenon was ascribed to the replacement of (bulkier) ClO_4^- ions, present in the

synthesis batch of IMO,[16] by (smaller) Cl^- ions deriving from the Fe precursor, with a consequent decrease of the interspace between adjacent NTs.[39] Formation of NTs is confirmed by HRTEM analysis: the reported micrographs concerning Fe-0.70-IMO sample show a bundle of NTs (Fig 3b) in a hexagonal array (Fig. 3c). N_2 isotherms (not reported) allowed measuring BET SSA and pores volume (Table 1): as a whole, the presence of Fe leads to an increase in surface area. The sample obtained by loading has a larger total volume: by difference with respect to micropores volume, mainly related to A pores, it results that the loading procedure mainly affected the outer surface of NTs.

The state of Fe is studied by means of DR-UV-Vis spectra in Figure 4a: similar curves are seen for the Fe-containing samples, whereas IMO (a white powder) weakly absorbs in the UV-Vis range. Both Fe-0.70-IMO and Fe-1.4-IMO mainly absorb at 270 nm; a minor absorption at 480 nm is clearly visible with Fe-1.4-IMO, but almost negligible with Fe-0.70.-IMO. Such results point out the occurrence of Al^{3+}/Fe^{3+} IS with both samples, since the band at 270 nm is due to charge-transfer transitions (CT) from O^{2-} to isolated octahedral Fe^{3+} sites, and of formation of iron oxo-hydroxide clusters at high Fe content, being the 480 nm band due to *d-d* transition of Fe_2O_3 clusters.[36,39] The spectrum of Fe-L-IMO, similar to that of Fe-1.4-IMO, is slightly shifted towards higher wavelengths, and more intense in the *d-d* transition range. Such result indicates that iron oxo-hydroxide cluster formation is favored by post-synthesis exchange, although Al^{3+}/Fe^{3+} IS also occurs.

The Tauc's plot in Figure 4b shows that IMO has a band-gap E_g = 4.9 eV, in agreement with the calculated value (4.6 eV).[34] Doping with Fe brings about a significant decrease of the band gap.

With Fe-0.70-IMO sample, where mostly IS Fe^{3+} species occur, E_g is 2.8 eV, indicating that Fe-doping has the effect of lowering the band gap, since the sample is approaching a semi-conductor behavior. With Fe-L-IMO, an even lower band gap is measured (E_g = 2.4 eV), although the presence of iron oxo-hydroxide clusters hampers a more precise determination of E_g in this sample.

The samples behavior in water is investigated by means of ζ-potential measurements and adsorption of $AO7^-$ from an aqueous solution at pH = 6.8. Since IR spectra reported elsewhere[39] did not notice relevant differences between IMO and Fe-0.70-IMO (due to the low Fe content), only the samples at 1.4 %wt. Fe content were considered. The ζ-potential curve of IMO (Figure 5a) shows that it is positively charged at low pH values, with a point of zero charge (PZC) at pH = 9.8, *i.e.* very close to that of alumina.[44,45] Fe-doped samples show a very similar behavior: the net difference in both surface charge and PZC among the samples is not relevant. As a whole, the samples are positively charged at low pH, and negatively charged at high pH, and therefore all of them should be able to adsorb anions and cations above and below their PZC, respectively.
$AO7^-$ adsorption results are reported in Figure 5b, as percentage of dye adsorbed as a function of time: the best performance is given by Fe-1.4-IMO, followed by IMO, indicating that the main process is electrostatic attraction between $AO7^-$ anions and the positively charged outer surface of the samples (the solution pH was 6.8).
However, some important differences are observed: Fe-1.4-IMO gives the best performance in terms of $AO7^-$ removal, with a steep increase in the dye adsorption in the very first minutes (accompanied by a pH drop, as reported in ref. 39). The same occurs, to a minor extent, also with Fe-0.70-IMO, because reaction (3) takes place:

$Fe(OH)_2^+Al + AO7^- = FeAO7^- + Al\text{-}OH + H^+$ (3)

which implies the formation of $FeAO7^-$ adducts, through a ligand displacement phenomenon, with N atoms of the dye coordinating IS Fe^{3+} sites.

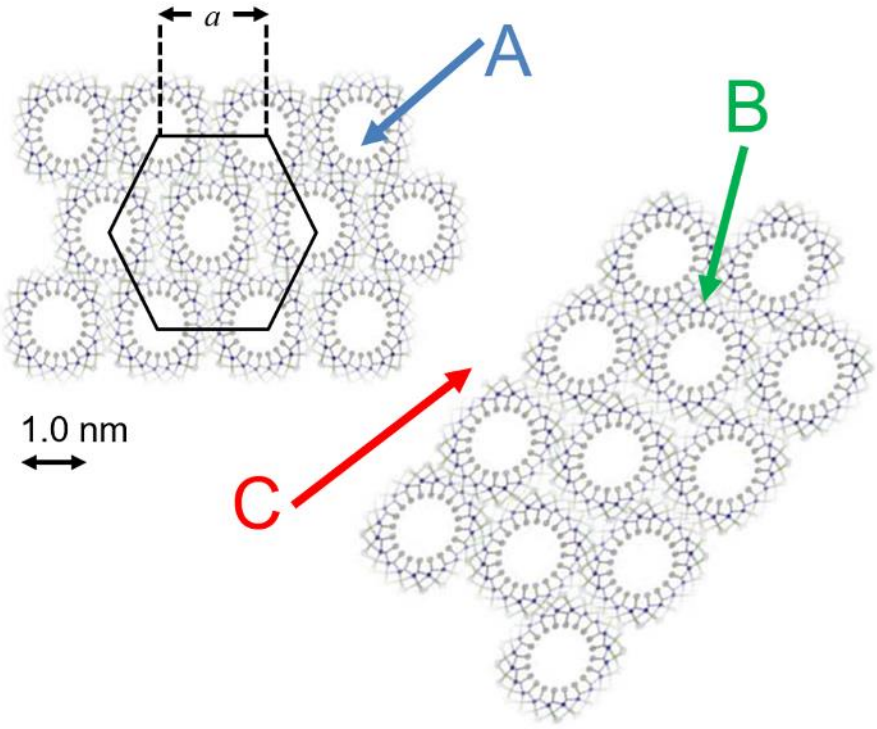

Figure 1. Representation of two bundles of IMO NTs in hexagonal packing. When occurring in powder form, IMO NTs are packed in bundles having nearly hexagonal symmetry. The cell parameter *a* evidenced in the Figure corresponds to the center-to-center distance between two aligned NTs within a hexagonal bundle. Pores A, B and C correspond to proper IMO nanopores (*ca.* 1.0 nm wide); nanopores among three aligned NTs (*ca.* 0.30-0.40 nm wide) and slit mesopores among bundles, respectively.

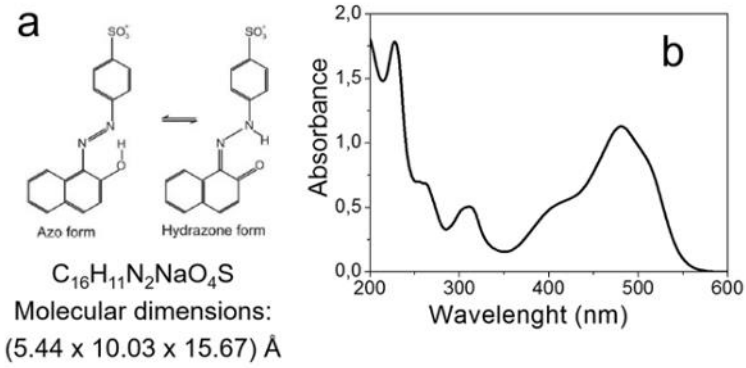

Figure 2. The azo-dye Acid Orange 7 in water: azo-hydrazone tautomerism and UV-Vis spectrum. Part (a) reports the chemical formula and molecular dimensions[42] of the dye along with its azo- and hydrazone forms, both present in water solution due to tautomerism. Part (b) reports the UV-Vis spectrum of the starting 0.67 mM solution of the dye used for the adsorption experiments.[39]

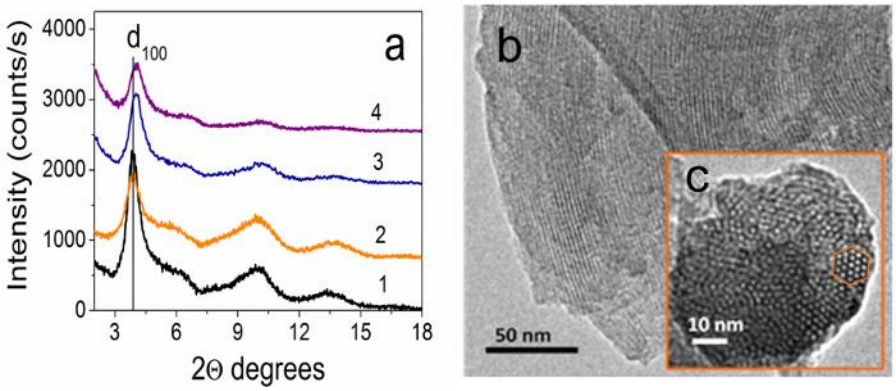

Figure 3. Textural characterization of the synthesized powder samples. Part (a) reports low angles XRD patterns of IMO (curve 1), Fe-L-IMO (curve 2), Fe-0.70-IMO (curve 3) and Fe-1.4-IMO (curve 4). Part (b) and (c) refer to sample Fe-0.70-IMO: a selected HRTEM micrograph of the powder sample is reported (b), along with a magnification of the frontal view of a bundle with NTs forming a hexagonal array (c).

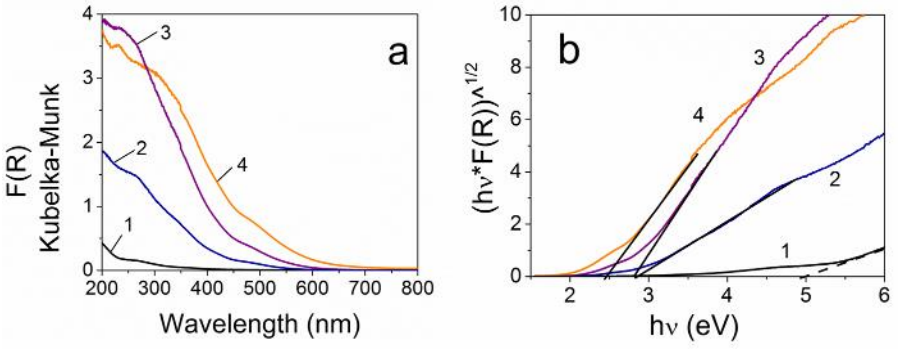

Figure 4 DR-UV-Vis spectroscopic characterization of the synthesized powder samples. Part (a) reports DR-UV-Vis spectra of IMO (curve 1), Fe-0.70-IMO (curve 2), Fe-1.4-IMO (curve 3) and Fe-L-IMO (curve 4). Part (b) reports the corresponding Tauc's plots, from which the bang-gap values (E_g, eV) reported in Table 1 were determined.

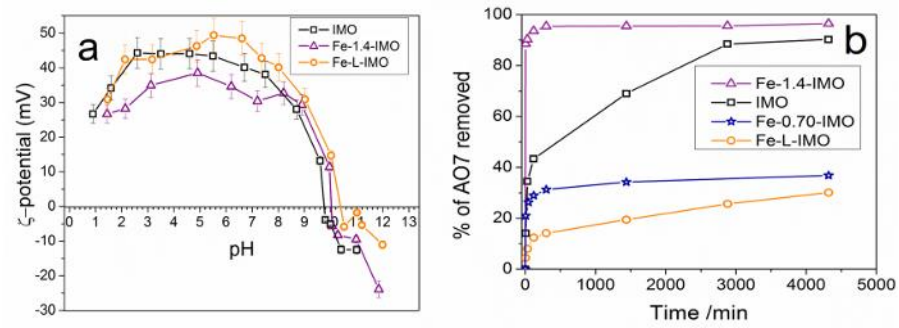

Figure 5 Measurements of samples surface charge and Acid Orange 7 adsorption experiments. Part (a) reports the ζ-potential curves of IMO (squares), Fe-1.4-IMO (triangles) and Fe-L-IMO (circles); error bars correspond to ±10% of the measured value, according to previous works.[38,39] Part (b) reports the percentage of $AO7^-$ removed versus time for IMO (squares), Fe-0.70-IMO (stars), Fe-1.4-IMO (triangles) and Fe-L-IMO (circles).

Sample	Fe, wt%	BET SSA (m^2g^{-1})	Total Volume (cm^3g^{-1})	Micropore Volume (cm^3g^{-1})	d_{100} (nm ± 0.01)	a (nm)	Band gap (eV)	PZC	$AO7^-$ removed
IMO	-	383	0.21	0.13	2.27	2.62	4.9	9.8	95 %
Fe-L-IMO	1.4	400	0.27	0.13	2.27	2.62	2.4	10.0	30 %
Fe-0.70-IMO	0.7	450	0.22	0.15	2.19	2.53	2.8	-	37 %
Fe-1.4-IMO	1.4	455	0.22	0.14	2.17	2.51	2.8	10.4	96 %

Table 1

Relevant properties of the samples, as determined by N_2 isotherms at -196 °C, XRD patterns, DR-UV-Vis spectroscopy, ζ-potential measurements and adsorption experiments with $AO7^-$ water solutions.

DISCUSSION

In order to be successful, the reported protocol has to be carefully followed, since formation of NTs strictly depends on the synthesis conditions. The following steps are critical: in steps 1.2 and 2.3 a slight excess of TEOS has to be used with respect to Si/Al stoichiometry ratio (i.e. TEOS: ATBS = 1.1 : 2). The excess of TEOS indeed prevents the preferential formation of

gibbsite ($Al(OH)_3$) and/or boehmite (AlOOH) phases.[46,47]

Another crucial point is the fast hydrolysis of ATBS: to prevent this, a moisture-free environment is needed, *e.g.* the dry-box adopted in this work. Within the dry-box, it is possible to measure the volumes of both TEOS and ATBS with graduated pipettes avoiding ATBS hydrolysis that would lead to an unsuccessful synthesis.

Another crucial point is dilution in step 1.6: at higher reagents concentration, condensation of orthosilicic acid would hinder the formation of NTs.

During polymerization, the temperature has to be controlled carefully. The temperature of polymerization during step 1.7 should not exceed 100 °C: to the best of our knowledge, the optimum range of temperature for polymerization in order to obtain a high yield of pure NTs is 95-100 °C. At lower temperatures, NTs formation rate decreases, whereas at higher temperatures other impurities (*e.g.* aluminum oxides) form.[48,49] The use of a thermostat would be the best solution, but measuring the temperature close to the autoclave within the stove may be enough, as done in this work.

The main limit of the synthesis protocol is that NTs do not form at Fe content higher than 1.4 wt. %, as also reported in the literature by authors using a slightly different protocol.[33] This can be due to some structural strains induced by Fe in this type of structures. The second main limit is the degree of Al^{3+}/Fe^{3+} IS that can be reached, corresponding to maximum 1.0 wt. % Fe. It has to be noticed, however, that the same was also observed with Fe-doped aluminogermanate NTs.[37]

On the contrary, the occurrence of IS also by post-synthesis loading is an interesting and encouraging result, likely related to the fact that Al(OH)Al groups at the outer surface of NTs are able to undergo ionic exchange in solution, according to reaction (4):

$[Al(OH)\ Al]_{(s)} + Fe(H_2O)_{6(aq)}^{3+} = [Fe(OH)\ Al]_{(s)} + Al(H_2O)_{6(aq)}^{3+}$ (4)

This result is particularly relevant and shows that the proposed protocol has important outcomes, since it opens to the possibility of changing the composition of IMO outer surface by ionic exchange, avoiding more complicated procedures, *i.e.* direct synthesis. As mentioned before, the synthesis of IMO requires several precautions to be successful and the mere addition of another reagent, in the present case $FeCl_3*6H_2O$, will perturb the synthesis environment. It is indeed simpler to add the Fe precursor to an aqueous solution of preformed NTs, as done for the Fe-L-IMO sample. The same procedure could be extended to other cations with proper charge and radius, like Cr^{3+} and Ti^{3+}. In the case of Ti^{3+}, however, there could be some limitation due to the stability of Ti^{3+} species and of its precursor.

Another important consequence of the successful doping procedure is the lowering of IMO band-gap: such result is particularly relevant if applications involving semiconductors are concerned, like photocatalysis. Moreover, the presence of reactive Fe^{3+} surface species could be exploited in photo-Fenton reaction for the removal of organic pollutants from water.

The formation of Fe(OH)Al groups, as a consequence of Al^{3+}/Fe^{3+} IS, provides Fe^{3+} sites that are accessible to species able to coordinate iron in water, as observed during $AO7^-$ adsorption experiments here reported. This concept could be extended to the retention of other organic pollutants, and so it would be possible to exploit the outer surface of NTs in adsorption processes involving not only mere electrostatic interaction, but ligand displacement, as well.

The worst performance of Fe-L-IMO towards $AO7^-$ adsorption is ascribable to the occurrence of a larger fraction of clusters: after addition of ammonia during loading, Cluster formation mostly occurs at the outer surface of NTs, as confirmed by pores volume reported in Table 1, showing

an increase of the total pore volume by loading, whereas the micropore volume, amenable to type A pores, remains unchanged. IS Fe^{3+} sites likely acted as crystallization centers for iron oxo-hydroxide clusters. Due to clusters formation, IS Fe^{3+} sites were no more accessible to $AO7^-$ species, finally lowering the adsorption capacity of Fe-L-IMO towards the dye.[39]

ACKNOWLEDGMENTS:

The authors acknowledge Prof. Claudio Gerbaldi (Politecnico di Torino) for lending the dry-box.

DISCLOSURES:

The authors have nothing to disclose.

REFERENCES

1. Ajayan, P.M. Nanotubes from carbon. *Chem. Rev*. **99 (7)**, 1787-1800, doi: 10.1021/cr970102g (1999).

2. Wada, S.I., Eto, A., Wada, K. Synthetic allophane and imogolite. *J. Soil. Sci.* **30 (2)**, 347–355, doi: 10.1111/j.1365-2389.1979.tb00991.x (1979).

3. Farmer, V.C., Adams, M.J., Fraser, A.R., Palmieri, F. Synthetic imogolite: properties, synthesis and possible applications. *Clay Miner.* **18 (4)**, 459–472, doi: 10.1180/claymin.1983.018.4.11 (1983).

4. Yoshinaga, N., Aomine, A. Imogolite in some ando soils. *Soil Sci. Plant Nutr.* **8 (3)**, 22–29, doi: 10.1080/00380768.1962.10430993 (1962).

5. Cradwick, P.D.G., Farmer, V.C., Russell, J.D., Wada, K., Yoshinaga, N. Imogolite, a Hydrated Aluminium Silicate of Tubular Structure. *Nature Phys. Sci.* **240**, 187–189, doi:10.1038/physci240187a0 (1972).

6. Bonelli, B., Bottero, I., Ballarini, N., Passeri, S., Cavani, F., Garrone, E. IR spectroscopic and catalytic characterization of the acidity of imogolite-based systems. *J. Catal.* **264 (2)**, 15–30, doi:10.1016/S0021-9517(02)00090-8 (2009).

7. Yang, H., Wang, C., Su, Z. Growth Mechanism of Synthetic Imogolite Nanotubes. *Chem. Mater.* **20 (13)**, 4484–4488, doi: 10.1021/cm8001546 (2008).

8. Wada, S. Imogolite synthesis at 25 °C. *Clay Clay Miner.* **35 (5)**, 379-384, doi: 10.1346/CCMN.1987.0350508 (1987).

9. Yucelen, G.I., Kang, D.-Y., Guerrero-Ferreira,R.C., Wright, E.R., Beckham, H.W., Nair, S. Shaping Single-Walled Metal Oxide Nanotubes from Precursors of Controlled Curvature. *Nano Lett.* **12**, 827-832, doi: 10.1021/nl203880z (2012)

10. Ackerman, W.C., Smith, D.M., Huling, J.C., Kim, Y., Bailey, J.K., Brinker, C.J. Gas/vapor adsorption in imogolite: a microporous tubular aluminosilicate. *Langmuir* **9 (4)**, 1051–1057, doi: 10.1021/la00028a029 (1993).

11. Wilson, M.A., Lee, G.S.H., Taylor, R.C. Benzene displacement on imogolite. *Clay Clay Miner.* **50 (3)**, 348–351, doi: 10.1346/00098600260358111 (2002).

12. Bonelli, B., Armandi, M., Garrone, E. Surface properties of alumino-silicate single-walled nanotubes of the imogolite type. *Phys. Chem. Chem. Phys.* **15 (32)**, 13381–13390, doi: 10.1039/C3CP51508G (2013).

13. Amara, M.S., Rouzière, S., Paineau, E., Bacia-Verloop, M., Thill, Al., Launois, P. Hexagonalization of Aluminogermanate Imogolite Nanotubes Organized into Closed-Packed Bundles, *J. Phys. Chem. C* **118**, 9299-9306, doi: 10.1021/jp5029678 (2014)

14. MacKenzie, K.J., Bowden, M.E., Brown, J.W.M., Meinhold, R.H. Structural and thermal transformation of imogolite studied by ^{29}Si and ^{27}Al high-resolution solid-stated magnetic nuclear resonance. *Clay Clay Miner.* **37 (4)**, 317-324, doi: 10.1346/CCMN.1989.0370404 (1989).

15. Kang, D. Y., Zang, J., Wright, E. R., McCanna, A. L., Jones, C. W., and Nair, S. (2010). Dehydration, dehydroxylation, and rehydroxylation of single-walled aluminosilicate nanotubes. ACS Nano 4, 4897–4907. doi:10.1021/nn101211y

16. Zanzottera, C., Vicente, A., Armandi, M., Fernandez, C., Garrone, E., Bonelli, B. Thermal collapse of single-walled aluminosilicate nanotubes: transformation mechanisms and morphology of the resulting lamellar phases. *J. Phys. Chem. C* **116 (13)**, 23577–23584, doi: 10.1021/jp301177q (2012).

17. Wada, S.I., Wada, K. Effects of Substitution of Germanium for Silicon in Imogolite. *Clay Clay Miner.* **30 (2),** 123–128, doi: 10.1346/ccmn.1982.0300206 (1982).

18. Thill, A., *et al.* Physico-Chemical Control over the Single-or Double-Wall Structure of Aluminogermanate Imogolite-like Nanotubes. *J. Am. Chem. Soc.* **134 (8)**, 3780–3786, doi: 10.1021/ja209756j (2012).

19. Mukherjee, S., Bartlow, V.M., Nair, S. Phenomenology of the growth of single-walled aluminosilicate and aluminogermanate nanotubes of precise dimensions. *Chem. Mater.* **17 (20)**, 4900–4909, doi: 10.1021/cm0505852 (2005).

20. Kang, D-Y., Zang. J., Jones, C.W., Nair, S. Single-Walled Aluminosilicate Nanotubes with Organic-Modified Interiors. *J. Phys. Chem. C* **115 (15)**, 7676–7685, doi: 10.1021/jp2010919 (2011).

21. Bottero, I. *et al.* Synthesis and characterization of hybrid organic/inorganic nanotubes of the imogolite type and their behaviour towards methane adsorption. *Phys. Chem. Chem. Phys.* **13 (2)**, 744–750, doi: 10.1039/C0CP00438C (2011).

22. Kang; D-Y., *et al.* Direct Synthesis of Single-Walled Aminoaluminosilicate Nanotubes with Enhanced Molecular Adsorption Selectivity. *Nature Commun.* **5**, 3342, doi:10.1038/ncomms4342 (2014).

23. Ma, W., Yah, M.O., Otsuka, H., Takahara, A. Application of imogolite clay nanotubes in organic-inorganic nanohybrid materials. *J. Mater. Chem.* **22 (24)**, 11887-11892, doi: 10.1039/C2JM31570J (2012).

24. Park, S. *et al.* Two-dimensional alignment of imogolite on a solid surface. *Chem. Commun.* 2917-2919, doi: 10.1039/B706505A (2007).

25. Yamamoto, K., Otsuka, H., Wada, S., Takahara, A. Surface modification of aluminosilicate nanofiber “imogolite”. *Chem. Lett.* **30**, 1162-1173, doi: 10.1246/cl.2001.1162(2001).

26. Zanzottera, C., Vicente, A., Celasco, E., Fernandez, C., Garrone, E., Bonelli, B. Physico-chemical properties of imogolite nanotubes functionalized on both external and internal surfaces. *J. Phys. Chem. C* **116 (13)**, 7499-7506, doi: 10.1021/jp301177q (2012).

27. Gustafsson, J.P. The surface chemistry of imogolite. *Clay Clay Miner.* **49 (1)**, 73-80, doi: 10.1346/CCMN.2001.0490106 (2001).

28. Denaix, L.; Lamy, I.; Bottero, J.Y. Structure and affinity towards Cd^{2+}, Cu^{2+}, Pb^{2+} of synthetic colloidal amorphous aluminosilicates and their precursors. *Coll. Surf. A* **158 (3)**, 315-325, doi: 10.1016/S0927-7757(99)00096-5 (1999).

29. Clark, C.J., McBride, M.B. Cation and anion retention by natural and synthetic allophane and imogolite. *Clay Clay Miner.* **32 (4)**, 291-299, doi: 10.1346/CCMN.1984.0320407 (1984).

30. Parfitt, R.L., Thomas, A.D., Atkinson, R.J., Smart, R. St.C. Adsorption of phosphate on imogolite. *Clay Clay Miner.* **22 (5-6)**, 455-456, doi: 10.1346/CCMN.1974.0220512 (1974).

31. Arai, Y., McBeath, M., Bargar, J.R., Joye, J., Davis, J.A. Uranyl adsorption and surface speciation at the imogolite-water interface: Self-consistent spectroscopic and surface complexation models. *Geochim. Cosmochim. Acta* **70 (10)**, 2492-2509, doi: 10.1016/j.gca.2006.02.013 (2006).

32. Harsh, J.B., Traina, S.J., Boyle, J., Yang, Y. Adsorption of cations on imogolite and their effect on surface charge characteristics. *Clay Clay Miner.* **40 (6)**, 700-706, doi: 10.1346/CCMN.1992.0400609 (1992).

33. Ookawa, M., Inoue, Y., Watanabe, M., Suzuki, M., Yamaguchi, T. Synthesis and characterization of Fe containing imogolite. *Clay Sci.* **12 (2)**, 280-284, doi: 10.11362/jcssjclayscience1960.12 (2006).

34. Alvarez-Ramírez, F. First Principles Studies of Fe-Containing Aluminosilicate and Aluminogermanate Nanotubes. *J. Chem. Theory Comput.* **5 (12)**, 3224-3231, doi: 10.1021/ct9004992 (2009).

35. Guimarães, L., Frenzel, J., Heine, T., Duarte, H.A., Seifert, G. Imogolite nanotubes: stability, electronic and mechanical properties. *ACS Nano* **1(4)**, 362-368, doi: 10.1021/nn700184k (2007).

36. Shafia, E. *et al.* Al/Fe isomorphic substitution versus Fe_2O_3 clusters formation in Fe-doped aluminosilicate nanotubes (imogolite). *J. Nanopar. Res.* **17 (8)**, 336, doi_ 10.1007/s11051-015-3130-2 (2015).

37. Avellan, A. *et al.* Structural incorporation of iron into Ge–imogolite nanotubes: a promising step for innovative nanomaterials. *RSC Advances* **4 (91)**, 49827-49830, doi: 10.1039/c4ra08840a (2014).

38. Shafia, E., Esposito, S., Armandi, M., Bahadori, E., Garrone, E., Bonelli, B. Reactivity of bare and Fe-doped alumino-silicate nanotubes (imogolite) with H_2O_2 and the azo-dye Acid Orange 7. *Catal. Tod.* DOI: 10.1016/j.cattod.2015.10.011.

39. Shafia, E., Esposito, S., Armandi, M., Manzoli, M., Garrone, E., Bonelli, Isomorphic substitution of aluminium by iron into single-walled alumino-silicate nanotubes: A physico-chemical insight into the structural and adsorption properties of Fe-doped imogolite. *Micropor. Mesopor. Mat.* **224**, 229-238, doi: 10.1016/j.micromeso.2015.11.044 (2016).

40. Arancibia-Miranda, N., Acuña-Rougiera, C., Escudey, M., Tasca, F. *Nanomaterials*, **6(2)**, 28, doi: 10.3390/nano6020028 (2016).

41. Freyria, F.S., Bonelli, B., Sethi, R., Armandi, M., Belluso, E., Garrone, E. Reactions of Acid Orange 7 with Iron Nanoparticles in Aqueous Solutions. *J. Phys. Chem. C* **115 (49)**, 24143-24152, doi: 10.1021/jp204762u (2011).

42. Zhao, X., Bu, X., Wu, T., Zheng, S.-T., Wang, L., Feng, P. Selective anion exchange with nanogated isoreticular positive metal-organic frameworks. *Nat. Commun.* **4,** 2344, doi: 10.1038/ncomms3344 (2013).

43. Bursill, L.A., Peng, J.L., Bourgeois, L.N. Imogolite: an aluminosilicate nanotube material. *Philos. Mag. A* **80 (1)**, 105-117, doi: 10.1080/01418610008212043 (2000).

44. Rotoli, B.M. *et al.* Imogolite: An Aluminosilicate Nanotube Endowed with Low Cytotoxicity and Genotoxicity. *Chem. Res. Toxicol.* **27 (7)**, 1142-1154, doi: 10.1021/tx500002d (2014).

45. Shu, H.-Y., Chang, M.-C., Hu, H.-H., Chen, W.-H. Reduction of an azo dye acid black 24 solution using synthesized nanoscale zerovalent iron particles. *J. Colloid Interface Sci.* **314 (1)**, 89-97, doi: 10.1016/j.jcis.2007.04.071 (2007).

46. Farmer, V.C. Synthetic imogolite, a tubular hydroxylaluminum silicate. International Clay Conference; 1978; Amsterdam, Netherlands: Elsevier.

47. Farmer, V.C., Fraser, A.R., Tait, J.M. Synthesis of imogolite: a tubular aluminium silicate polymer. *J. Chem. Soc. Chem. Commun.* **13,** 462-463, doi: 10.1039/c39770000462 (1977).

48. Violante, A., Huang, P.M. Formation mechanism of aluminum hydroxide polymorphs. *Clay Clay Miner*. **41(5)**, 590-597, doi: 10.1346/CCMN.1993.0410509 (1993).

49. Violante, P., Violante, A., Tait, J.M. Morphology of nordstrandite. *Clay Clay Miner*. **30(6)**, 431-437 doi: 10.1346/CCMN.1982.0300605 (1982).